Capturing Contact in Mitral Valve Dynamic Closure with Fluid-Structure Interaction Simulation

Nariman Khaledian, Pierre-Frédéric Villard, Marie-Odile Berger

Capturing Contact in Mitral Valve Dynamic Closure with Fluid-Structure Interaction Simulation

Nariman Khaledian[1*], Pierre-Frédéric Villard[1†] and Marie-Odile Berger[1†]

[1*]Université de Lorraine, CNRS, Inria, LORIA, Nancy, France.

*Corresponding author(s). E-mail(s): nariman.khaledian@inria.fr;
Contributing authors: pierrefrederic.villard@loria.fr;
marie-odile.berger@inria.fr;
†These authors contributed equally to this work.

Abstract

Purpose: Realistic fluid-structure interaction (FSI) simulation of the mitral valve opens the way toward planning for surgical repair. In the literature, blood leakage is identified by measuring the flow rate but detailed information about closure efficiency is missing. We present in this paper an FSI model that improves the detection of blood leakage by building a map of contact. **Methods:** Our model is based on the immersed boundary method that captures a map of contact and perfect closure of the mitral valve, without the presence of orifice holes, which often appear with existing methods. We also identified important factors influencing convergence issues. **Results:** The method is demonstrated in three typical clinical situations: mitral valve with leakage, bulging, and healthy. In addition to the classical ways of evaluating MV closure, such as stress distribution and flow rate, the contact map provides easy detection of leakage with identification of the sources of leakage and a quality assessment of the closure. **Conclusion:** Our method significantly improves the quality of the simulation and allows the identification of regurgitation as well as a spatial evaluation of the quality of valve closure. Comparably fast simulation, ability to simulate large deformation, and capturing detailed contact are the main aspects of the study.

Keywords: FSI, Mitral valve, Contact, Biomechanical simulation

1 Introduction

The mitral valve (MV) of the heart ensures blood one-way flow from the left atrium to the left ventricle. Many pathologies damage the valve anatomy potentially leading to heart failure. Such cases could be treated by surgical repair of the valve. Currently, the surgeon must predict the surgery outcome, and the results are highly dependent upon the surgeon's experience. Numerical analysis such as Fluid-structure interaction (FSI) simulation can help with a better understanding of mitral valve dynamic motion and later simulate patient-based procedures such as surgical treatment planning.

Various works have studied MV behavior without including fluid mechanics [1, 2], but they only focus on peak systole at the static state. Their aim is not to examine the complex dynamic motion nor to simulate blood leakage through the valve. FSI simulation of the MV is a challenging non-linear problem due to the complex geometry of the MV, self-contact existing in multiple regions, and the large deformations undergone during closure. Many studies in the literature [3–5] focused on different aspects of MV FSI simulation, without considering numerical ways to obtain an accurate and realistic simulation of the valve closure. We are interested in methods that can perform biomechanic simulation of MV closure and are able to reproduce the expected behavior of healthy MV, and MV with pathological diseases, such as bulging and regurgitation.

The structure is represented by the traditional Lagrangian domain, where the deformations in the material change the mesh representation. The numerical representation of the fluid can be done by Eulerian mesh, Lagrangian mesh, or a mix between the two. In the Eulerian representation, blood flow is measured at a fixed set of points like in the Immersed Boundary (IB) method. Two methods use a pure or mixed Lagrangian representation for the fluid: smooth particle hydrodynamics (SPH) and Arbitrary Lagrangian-Eulerian (ALE). Pros and cons of these techniques are described below.

A simple FSI technique widely used in the studies of the MV [3, 5], is SPH. The Lagrangian mesh representation of the SPH made it suitable for capturing contact in the FSI simulations. However, specifying boundary conditions in the SPH is difficult and the particle-based nature of the SPH made this technique highly computationally intensive.

With ALE, the fluid domain is represented with the mix of Eulerian and Lagrangian mesh representation, where the blood can flow through the domain and the fluid mesh is impacted by the structure's deformation. This allows for the structure boundaries in the fluid domain to be sharply defined. In ALE, the contact between two surfaces may crush the fluid cells to zero and result in a disconnected fluid domain and negative cell volumes [6] (see Fig. 1a).

The IB approach, with the Eulerian mesh representation in the fluid domain, addresses this issue by defining no structure boundaries in the fluid domain. This means that borders of the MV geometry are not connected to the blood mesh and they can freely deform without changing the blood mesh. In IB methods, the structure domain occupies void regions inside the fluid

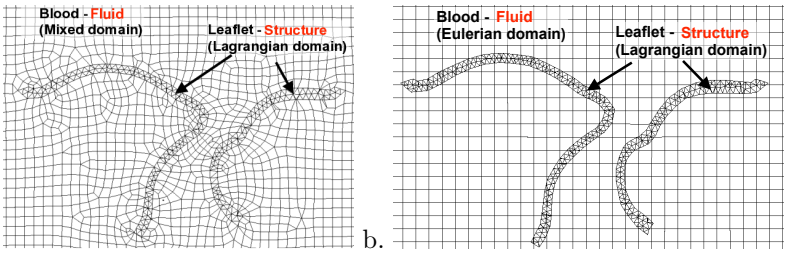

a. b.

Fig. 1 ALE (*a.*) and IB (*b.*) mesh representation of MV leaflet inside blood

domain. The contact algorithm automatically computes and tracks the interface between MV and blood. Contact constraints between blood and MV are enforced using a penalty method, where the default penalty stiffness parameter is automatically maximized subject to stability limits. In IB, there is no need to generate a conforming mesh for the fluid domain. Instead, a simple mesh ([7]) generally produces the best accuracy (see Fig. 1b).

The ALE technique is capable of better capturing the interface between the blood and leaflets [8], but the blood mesh representation in IB is independent of MV deformation. IB allows to capture a precise contact between leaflets, eliminates the ALE stability issues related to the blood domain caused by the dynamic mesh, remove the computational cost of dynamic mesh, and facilitate the simulation of the large deformation of leaflets. Based on these characteristics, we decided to implement IB techniques.

Addressing contact models in the FSI framework has been previously studied in the literature [9, 10]. In [6], contact behavior in IB and ALE approaches are compared. They observed numerical instabilities, with solutions never converging for 3D simulation of contacts in ALE. In [8] ad hoc techniques were used to capture contacts: once the leaflets reached a distance threshold from each other, the fluid was blocked by constraints resulting in a small gap where both surfaces should match. In general, determining a perfect closure of MV, and having detailed information about the contact area in the leaflets, which has great importance in clinical applications, have not been studied in the literature. The frameworks presented in [4, 5, 11] exhibit contacts but lack either a detailed description of the contact models and/or do not give ways to evaluate the quality of the contacts. Moreover, relatively large orifice holes appear in the fully closed state of the MV and are not explained.

In this study, we propose an FSI framework based on IB including a model that can capture details of contact between MV leaflets with a focus on two important issues. One is the closure of MV without leakage and zero orifice holes by reducing convergence issues and implementation of a proper contact model. We addressed the issue of numerical instability by including practical information about the MV case setup in the FSI simulation. The other is a contact evaluation technique to identify contact areas in MV leaflets and detect blood leakage. In case of no leakage, the magnitude of the contact force in each

area can give information about the quality of contact. This information can help the surgeon to find weak spots which are likely to produce blood leakage.

The rest of the paper is organized as follows: In section 2, we present the overall biomechanical model. Important aspects of the model necessary for capturing contact and reducing convergence issues with low computational cost are also discussed. Results of typical clinical situations are shown in section 3.

2 Methods

The MV geometry can be extracted from 3D medical images, in a manual or semi-automatic way. Instead, we work on a generic MV that encompasses many difficulties encountered in real cases. The generic valve is constructed from a 2D geometry containing four semicircles arranged in a row then wrapped into a cone with an elliptic base (see Fig. 2b).

2.1 Model configuration

The MV is immersed inside a blood domain, with chordae endpoints connected to a fixed node located on a papillary muscle and to the leaflet. The annulus nodes are fixed to the ventricular wall. No-slip boundary conditions, i.e. a zero blood velocity relative to the surface, are considered on the leaflets as well as the tube wall, which is the common way to model the fluid-structure interface. The blood is simulated as an incompressible, isothermal, and Newtonian fluid with a dynamic viscosity of $2e^{-3}Pa.s$ and density of $1060kg/m^3$. A friction coefficient of 0.2 for the shear contact between leaflets is used. Time-dependent transvalvular pressure based on real measurements extracted from [12] is applied on the bottom of the fluid domain to simulate the pressure difference between the left ventricle and left atrium. The simulation starts from the systolic peak and continues until the diastolic peak in the cardiac cycle. Depending on the residuals, an adaptive time step, with the initial time step of $4e^{-4}$, is used. The average time step is $3.6e^{-4}$ with the minimal time step of $1e^{-4}$. All the boundary conditions are displayed in Fig. 2b.

Chordae: The chordae structure is modeled as a linear elastic beam (see Fig. 2b) with a constitutive model based on experimental data [13]. Due to the challenges in MV geometry acquisition, and the complex structure in chordae attachment to the leaflets, no study was able to accurately extract the chordae structure in the region near the leaflets or find the attachment points of the chordae to the leaflets. A common technique used in the literature is to use a sphere of influence near the chordae extremities [14]. For each chordae attachment, a gradually decreasing distribution of the chordae forces over a group of leaflet nodes avoids the concentration of forces over a single node and potentially prevents element distortion. This also reduces the degree of freedom of leaflet nodes with respect to the chordae endpoint. Since the amplitude of chordae forces is larger for chordae with no bifurcation, we use two influence sphere sizes (R and $R/2$), where R is on the order of the leaflet width, to handle the two types of chordae. Connecting only the inner surface of the leaflets

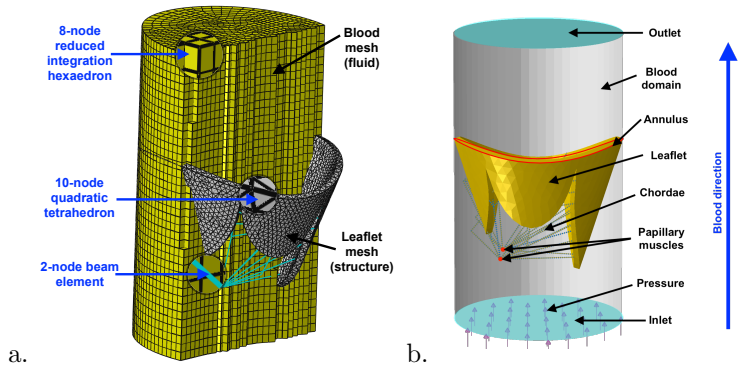

Fig. 2 Biomechanical modeling. *a.* mesh partition *b.* anatomy and boundary conditions

to chordae results in shear stress through the leaflet thickness, which causes element distortion. By contrast, involving nodes on both sides of the leaflet thickness eliminates the unnecessary shear tension and reduces the excessive deformation in the elements.

Leaflets: To simplify the problem, we specified a uniform leaflet thickness and neglected its anisotropic behavior. The leaflet is modeled as a homogeneous incompressible 3rd order Ogden hyperelastic material with coefficients based on experimental data [15]. For the leaflet, a 10-node quadratic tetrahedron element is used (see Fig. 2a). Complex deformations of MV may potentially lead to negative element volumes, where node alignments in the element may exhibit skewness or asymmetric deformation. We thus used a penalty-based element distortion approach to make large deformations possible. In this technique, elements are monitored for distortion, and once the strain in a specific element reaches a certain percentage of its nominal strain, the material behavior of the deformed element stiffens significantly. Based on our observations, element distortion control only involves a small number of elements (less than 1% percent) during the MV closure, where wrinkles on the leaflet occur. Therefore, the effect of distortion control on the overall stiffness of the structure is negligible. This technique, in combination with a fine mesh, prevents elements to become non-convex and generate negative element volumes, which is the cause for the majority of convergence issues in large deformation simulations.

Blood: For the blood domain, linear 3D elements, generated by 8-node reduced integration are implemented. For better visualization, only half of the fluid domain is represented in Fig. 2a. Using reduced integration will lower the computational cost. Stiffness and viscosity factors are applied as regularization by the hourglass control [16] to guarantee a negligible impact on the mechanical accuracy.

2.2 Contact model

Literature on contacts in mechanics is rich. Our objective is to select appropriate contact models that are suited to MV and allow proper simulation in

typical clinical cases with a specific focus on a sealed closure. Reducing computational issues and ensuring convergence of the simulation process has also guided these choices. It must be noted that when only the structural analysis is considered (without fluid coupling), numerical stability can be easily obtained [2]. However, capturing contact in MV dynamic closure, with the FSI context, produces closure with orifice holes and gives rise to instabilities or divergence.

In our FSI model, both perpendicular and frictional contacts between leaflets are considered, contrary to existing works which used friction-less contact models [2, 9] and did not explicitly mention the used contact model and exhibit orifice holes [3, 4, 11]. In the following, the main attributes of capturing contact that impact the computation cost and convergence of the model are presented first on the leaflets to model self-contacts and secondly on the fluid-structure interface to allow FSI coupling.

Leaflet self-contacts: Self-contacts are handled with a balanced master-slave technique. This technique applies master-slave formulation twice, each time selecting one of the two surfaces in contact as a master and the other one as a slave. In this technique, contrary to classical contact models, the correction forces on both surfaces are equally weighted, which is suitable for surfaces with similar mesh properties and physical characteristics.

At each time instant, continuous tracking of nodes that are in contact is realized based on a threshold distance [17]. If this distance is negative, penetration occurs and the goal of the contact model is to apply a counterforce in the direction of the normal to the surface [2, 6]. Surfaces in contact also transmit shear in addition to normal forces across their interface. Frictional contacts are thus added as a tangential component. Handling contact operates in a two steps loop:

1. Computation of the normal force F_n with a penalty-based method [18]. Though kinematic allows more accurate contacts, they are often prone to divergence. Penalty-based method reduce over-constraints and lead to lower computation time. The tangential component f is computed based on Coulomb's friction model $f = \mu F_n$, where μ is the friction coefficient.
2. The nodes displacement are estimated based on the equation of motion of the whole system that links the external, internal, and contact forces to the acceleration $\gamma : F_{ext} + F_{int} + f + F_n = m\gamma$.

In order to save time, identification of the nodes in contact is realized once every four iterations. In order to decrease the penetration of the two surfaces, averaging the minimum distance of a slave node to master facets in a neighboring region is performed instead of the classical node to node distance.

Fluid-structure interface: The balanced master-slave formulation with penalty constraints is used to capture contacts between blood and leaflets. More detailed information on the penalty constraint method is presented in [7]. In IB techniques, the fluid mesh is fixed and independent of the deformation

of leaflets. This results in accurate closure of MV by allowing the leaflets to be in contact without creating negative cell volumes in the fluid domain.

3 Results

We propose here to quantitatively measure the MV dynamic closure in the systole phase. Simulation results are provided in different typical medical configurations: MV with no chordae, leakage, bulging, and healthy MV. These results show the ability of our model to reproduce the expected MV behavior. We did a mesh resolution independency study by comparing the results of stress distribution over leaflets. The mesh resolution with less than one percent difference in accuracy is selected for the simulation purpose. Both fluid and solid domains are simulated at the same time in Abaqus explicit solver with contact formulation of fluid and solid domain based on an enhanced immersed boundary method [7].

Time: MV was meshed with 71k elements in the fluid domain and 20k elements for the leaflet, which produces a two-layered mesh, in the structure domain. The simulation took 8 hours on Intel Xeon 3.60 GHz workstation with 12 processors. With respect to the FSI studies of MV in the literature, for example, five days of computation time in [5], and 18 hours of computation time in [19], still with mesh independency being satisfied, the framework we presented in this study is comparably faster.

Deformed shape: A first step in qualitatively evaluating the outcome of the FSI simulation is observing the deformed geometry at the end of the simulation. Videos of the whole dynamic deformation for each case study are available with the article. The closed state of the MV in the four different scenarios has been studied. Fig. 3.a shows the results with no chordae holding the leaflets to test the simulation. It checks if the mechanical modeling and particularly the constitutive law allows the valve to completely open and checks if it is not overly constrained. Closure of MV with leakage is shown in Fig. 3.b. MV closure with blood leakage is replicated by removing 4 primary chordae from the total 14 primary chordae attached to the border of the leaflets to create a large orifice hole in the structure. In Fig. 3.c, MV with severe bulging is shown. The bulging is replicated by removing chordae that hold the inner region of the anterior leaflet. These two behaviors can be compared with the MV in a healthy state (Fig. 3.d). We have replicated this simulation with a real porcine heart that emerged in a water tank and where pressure was applied through a pump[1]. Though the considered geometry in the real and the simulated case are not identical, similar behavior is observed: similar acceleration during closure and a slight back-and-forth lateral motion near the end.

Stress map: Another common way to check qualitatively the validity of the simulation is to analyze the stress map by displaying the Von Mises distribution. Stress distribution in different scenarios is presented in Fig. 4. A

[1]Slow-motion video of mitral valve closure: https://hal.archives-ouvertes.fr/hal-03419776

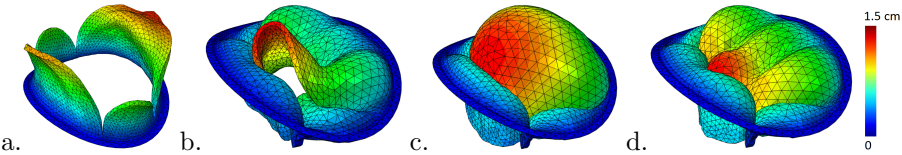

Fig. 3 Displacement of MV with *a.* no chordae *b.* leakage *c.* bulging and *d.* perfect closure

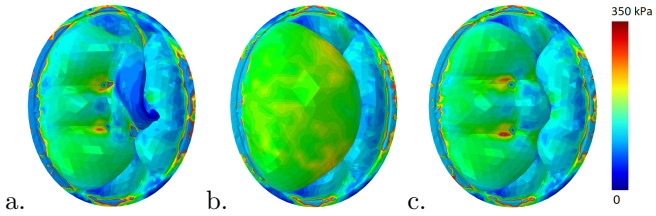

Fig. 4 Stress distribution of leaflets with *a.* leakage *b.* bulging and *c.* perfect closure

relatively large difference in stress distribution can be observed by comparing the results from healthy MV (Fig. 4c) and MV with bulging (Fig. 4b). MV leaflets in the bulging case experience a higher stress range in each cycle. These results are in accordance with clinical observations, in which bulging adds unnecessary force and more fatigue to the MV. In both healthy MV and MV with leakage (Fig. 4b), the maximum stress pattern is in agreement with other studies in the literature [4, 11, 20].

Streamlines: Streamlines are commonly used in the literature to analyze the fluid behavior [11, 20]. Fig. 5 shows the flow pattern with streamlines initiating from a segment at the inlet. The streamlines for the no chordae configuration (Fig. 5a) show the fluid going straight to the outlet as expected. No blood leakage is visible in the case of healthy (Fig. 5d) and bulging (Fig. 5c) MV, and in MV with leakage, streamline of blood leakage through the orifice hole is visible in Fig. 5b. The blood flow through the orifice hole has a higher velocity which creates jet flows penetrating the MV closing area. In the case of MV closure with bulging, different high momentum flow patterns appear in comparison with the healthy MV closure. This difference is due to the cavity region created by the severe deformation of the MV anterior leaflet. However, in both cases, the Reynolds number reach a value above 2000 (with a maximum of 28000) and in some regions, the chaotic breakdown of vortices occurs.

Cross-section in the contact region: In order to better appreciate the quality of the contact region between both leaflets, cross-sections of leaflets in the three case setups are compared in Fig. 6a. In both healthy and bulging cases, as expected, contact between leaflets occurs. The shape of leaflets in the healthy MV is relatively flat as a clinical sign of a healthy valve. In the case of bulging, a large balloon-shaped deformation is visible which causes high-stress loading on the leaflets in each cycle. The orifice area in the case of leakage is appearing as a gap that allows for blood to pass through the MV.

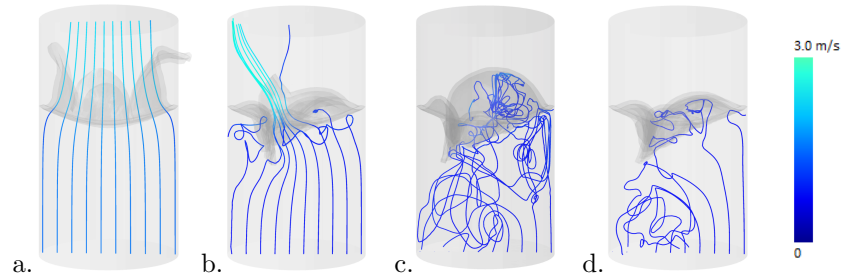

Fig. 5 Streamlines over MV with *a.* no chordae *b.* leakage *c.* bulging and *d.* perfect closure

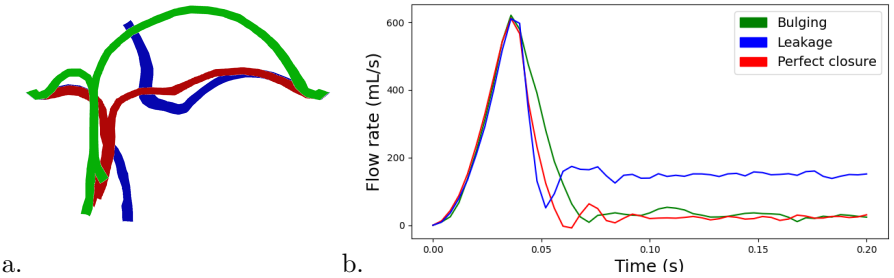

Fig. 6 *a.* Cross section and *b.* flow rate over time of MV with bulging, leakage and perfect closure

Flow rate: In several FSI studies including [4, 11, 20], the flow rate is used to measure the proper closure of the MV. Fig. 6b exhibits flow rate results: as expected, flow rates decay to zeros for the healthy and bulging cases. In the case of leakage, the flow rate reaches a certain value depending on the severity of the regurgitation. The resolution of the fluid mesh may influence the estimated flow rate. However, testing the method with 80k,100k and 280k mesh size produces 26.2, 23.9, and 22.6 as flow rates after closure and shows therefore a negligible influence on the whole process.

Unfortunately, this metric is not sufficiently sensitive to accurately measure leaks or identify holes. Indeed the ratio of leaks or holes areas is very small with respect to the leaflet areas, thus leading to near zeros flow rates. For example in [20], the flow rate for the cardiac cycle reaches zero despite the orifice areas in the simulation. For these reasons, we propose to evaluate the quality of the closure based on the contact map.

Contact map: To accurately detect the leakage in the MV, contact forces applied on the deformed leaflet nodes are associated with the node coordinates in the undeformed shape of the MV. To have a comprehensive map of unfolded leaflets, these data are mapped on a 2D figure to be visualized (see Fig. 7). The source of leakage can be accurately detected by observing the discontinued regions on the contact map. Fig. 7a shows the unfolded map of leaflets mesh where the contact forces are computed. In the case of healthy MV (Fig. 7b), non-zero contact forces in the contact map create a continuous belt without

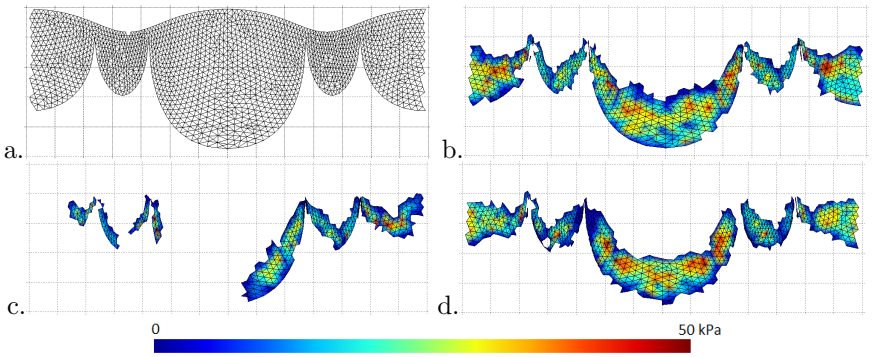

Fig. 7 Contact map: *a.* MV leaflets *b.* perfect closure *c.* leakage *d.* bulging

interruption. This will guarantee zero orifice holes in the leaflets and blood can not pass through the MV. In case of leakage (Fig. 7c), a large gap in the contact belt shows the presence of orifice holes. The location of the orifice holes shows the source of blood leakage. A small discontinuity appears in the contact map in the case of MV with bulging (Fig. 7d), which is a sign of a closure that is not perfect. This small gap is difficult to spot in the simulation results and in the flow rate but it can be easily detected with the help of the contact map. Furthermore, the width of the contact belt is different in both cases of healthy and bulging which shows different closure qualities. In terms of clinical application, the thickness of the region in contact and the magnitude of the contact force are valuable information that can help the surgeon identify the spots with weak contact and take measures in advance.

4 Conclusion and discussion

The main focus of this study is to capture detailed contact in the FSI simulation of MV, based on the IB method, and analyze the influence of contact model parameters on the dynamic closure of MV. Our model is able to reproduce different pathological cases and even simulation with no chordae that shows high numerical stability of the model. Faithfully capturing contacts with a relatively low computational cost is an important attribute of our model.

We evaluated the quality of the dynamic closure of MV with different measurements such as stress map, cross-sections, and flow rate. We also introduced a new method for evaluating the quality of the dynamic closure of MV. Contact map significantly improves the detection of MV dysfunctions. It can be used to identify regions with poor contact quality to predict pathological diseases. Using geometry extracted from 3D medical images, implementing anisotropic behavior of the constitutive model, and reducing the computation time further with techniques such as adaptive re-meshing in the regions that need more refinement, are ongoing research to improve our model.

Declarations

Conflict of interest: The authors declare that they have no conflict of interest.

References

[1] Panicheva, D., Villard, P.-F., Hammer, P.E., Perrin, D., Berger, M.-O.: Automatic extraction of the mitral valve chordae geometry for biomechanical simulation. International Journal of Computer Assisted Radiology and Surgery **16**(5), 709–720 (2021)

[2] Hammer, P.E., Pedro, J., Howe, R.D.: Anisotropic mass-spring method accurately simulates mitral valve closure from image-based models. In: International Conference on Functional Imaging and Modeling of the Heart, pp. 233–240 (2011). Springer

[3] Toma, M., Einstein, D.R., Bloodworth IV, C.H., Cochran, R.P., Yoganathan, A.P., Kunzelman, K.S.: Fluid–structure interaction and structural analyses using a comprehensive mitral valve model with 3d chordal structure. International journal for numerical methods in biomedical engineering **33**(4), 2815 (2017)

[4] Cai, L., Wang, Y., Gao, H., Ma, X., Zhu, G., Zhang, R., Shen, X., Luo, X.: Some effects of different constitutive laws on fsi simulation for the mitral valve. Scientific Reports **9**(1), 1–15 (2019)

[5] Caballero, A., Mao, W., McKay, R., Primiano, C., Hashim, S., Sun, W.: New insights into mitral heart valve prolapse after chordae rupture through FSI computational modeling. Scientific reports **8**(1), 1–14 (2018)

[6] Bavo, A.M., Rocatello, G., Iannaccone, F., Degroote, J., Vierendeels, J., Segers, P.: FSI simulation of prosthetic aortic valves: comparison between immersed boundary and arbitrary lagrangian-eulerian techniques for the mesh representation. PloS one **11**(4), 0154517 (2016)

[7] Benson, D.J.: Computational methods in lagrangian and eulerian hydrocodes. Computer Methods in Applied Mechanics and Engineering **99**(2), 235–394 (1992)

[8] Hiromi Spühler, J., Hoffman, J.: An interface-tracking unified continuum model for fluid-structure interaction with topology change and full-friction contact with application to aortic valves. International Journal for Numerical Methods in Engineering **122**(19), 5258–5278 (2021)

[9] Astorino, M., Gerbeau, J.-F., Pantz, O., Traoré, K.-F.: Fluid–structure interaction and multi-body contact: Application to aortic valves. Computer Methods in Applied Mechanics and Engineering **198**(45), 3603–3612

(2009)

[10] van Loon, R., Anderson, P.D., van de Vosse, F.N.: A fluid–structure interaction method with solid-rigid contact for heart valve dynamics. Journal of Computational Physics **217**(2), 806–823 (2006)

[11] Feng, L., Qi, N., Gao, H., Sun, W., Vazquez, M., Griffith, B.E., Luo, X.: On the chordae structure and dynamic behaviour of the mitral valve. IMA journal of applied mathematics **83**(6), 1066–1091 (2018)

[12] Levick, J.R.: An Introduction to Cardiovascular Physiology. Butterworth-Heinemann, Oxford (2013)

[13] Millard, L., Espino, D.M., Shepherd, D.E., Hukins, D.W., Buchan, K.G.: Mechanical properties of chordae tendineae of the mitral heart valve: Young's modulus, structural stiffness, and effects of aging. Journal of mechanics in medicine and biology **11**(01), 221–230 (2011)

[14] Drach, A., Khalighi, A.H., Sacks, M.S.: A comprehensive pipeline for multi-resolution modeling of the mitral valve: Validation, computational efficiency, and predictive capability. International journal for numerical methods in biomedical engineering **34**(2), 2921 (2018)

[15] May-Newman, K., Yin, F.: Biaxial mechanical behavior of excised porcine mitral valve leaflets. American Journal of Physiology-Heart and Circulatory Physiology **269**(4), 1319–1327 (1995)

[16] Belytschko, T., Ong, J.S.-J., Liu, W.K., Kennedy, J.M.: Hourglass control in linear and nonlinear problems. Computer Methods in Applied Mechanics and Engineering **43**(3), 251–276 (1984)

[17] Yang, B., Laursen, T.A.: A large deformation mortar formulation of self contact with finite sliding. Computer Methods in Applied Mechanics and Engineering **197**(6), 756–772 (2008)

[18] Belytschko, T., Neal, M.O.: Contact-impact by the pinball algorithm with penalty and lagrangian methods. International Journal for Numerical Methods in Engineering **31**(3), 547–572 (1991)

[19] Lau, K.D., Diaz, V., Scambler, P., Burriesci, G.: Mitral valve dynamics in structural and fluid–structure interaction models. Medical Engineering & Physics **32**(9), 1057–1064 (2010)

[20] Gao, H., Ma, X., Qi, N., Berry, C., Griffith, B.E., Luo, X.: A finite strain nonlinear human mitral valve model with fluid-structure interaction. International journal for numerical methods in biomedical engineering **30**(12), 1597–1613 (2014)